



Mapping Spatial Distribution Characteristics of Lineaments Extracted from Remote Sensing Image Using Fractal and Multifractal Models

Cheng Lyu ^{*1,2}, Qiuming Cheng^{1,2}, Renguang Zuo¹, Xueping Wang²

1. State Key Laboratory of Geological Processes and Mineral Resources, China University of Geosciences, Wuhan 430074, China

2. Faculty of Earth Resources, China University of Geosciences, Wuhan 430074, China

 Cheng Lyu: <http://orcid.org/0000-0003-3094-0311>

ABSTRACT: Mapping mineral prospectivity in vegetated areas is a challenge. For this reason, we aimed to map spatial distribution characteristics of linear structures detected in remote sensing images using fractal and multifractal models. The selected study area was the Pinghe District of the Fujian Province (China), located in the Shanghang-Yunxiao polymetallic and alunite ore belt (within the Wuyishan polymetallic belt), where mineral resources such as copper, molybdenum, gold, silver, iron, lead, zinc, alunite and pyrophyllite have been discovered. The results of our study showed that: (1) the values of fractal dimension for all lineaments, NW-trending lineaments, and NE-trending lineaments, are 1.36, 1.32, and 1.23, respectively, indicating that these lineaments are statistically self-similar; (2) the fractal dimensions of the spatial distribution of the linear structures in the four selected hydrothermal-type ore deposits of the Pinghe District, named Zhongteng, Panchi, Xiaofanshan and Fanshan, are 1.43, 1.52, 1.37 and 1.37, respectively, which are higher than the mean value in South China; (3) the spatial distribution of the linear structures extracted from the remote sensing image and displayed by the contour map of fractal dimensions, correlates well with the known hydrothermal ore deposits; and (4) the results of the anomaly map decomposed by the spectrum-area (S-A) multifractal model is much better than the original fractal dimension contour map, which showed most of the known hydrothermal-type deposits occur in the high anomalous area. It is suggested that a high step tendency possibly matches with the boundary of the volcanic edifice and the deep fault controlling the development of the rock mass and the volcanic edifice. The complexity of the spatial distribution of mapped lineations (faults) in the Pinghe District, characterized by high values in the anomaly map, may be associated with the hydrothermal polymetallic ore mineralization in the study area.

KEY WORDS: fractal model, ETM+ data, vegetation coverage area, Pinghe molybdenum deposit.

0 INTRODUCTION

Existing studies show that most of the linear structures in remote sensing images reflect the stress produced by rock deformation belts or stress concentration belts (Ma and Xu, 1999). Consequently, the spatial distribution of faults in vegetated areas could be extracted from the linear structures in remote sensing images, which is a practical, low-cost, efficient, and fast technology. Faults can provide the pathway for hydrothermal fluids, resulting in significant metal depositional sites. However, irregularities in the linear structures often render the study of their spatial aspects difficult. The analyses of linear structures, including length, density and orientation, cannot

adequately reflect their complex spatial distribution (Zhao S et al., 2011).

Since Mandelbrot founded the fractal theory in the mid-1970s, the fractal geometry has been widely used in earth science as a new scientific and practical method to study remote sensing lineaments for mineral exploration (Yu and Yuan, 2005). In the past few decades, the application of fractal geometry in quantitative descriptions of natural phenomena, especially of spatial distribution of mineral deposits, has been developed (Zhao J N et al., 2011). Fractal statistical analysis has been demonstrated as a useful tool for identifying irregularities in the patterns of natural objects and for describing self-similarities in geological surveys (Ke et al., 2015; Gumiel et al., 2010; Zuo et al., 2009, 2008; Cheng et al., 1996, 1994; Carlson, 1991; Mandelbrot, 1983). Fractal analyses have also been used to interpret the relationships between linear structures from remotely sensed images and mineral deposits, which are with the geological map using concentration-area (C-A) fractal model based on remote sensing data (Aramesh Asl et al., 2015). A correlation

*Corresponding author: chenglyu85@gmail.com

© China University of Geosciences and Springer-Verlag Berlin Heidelberg 2017

Manuscript received June 30, 2016.

Manuscript accepted October 9, 2016.

between remote sensing data and geochemical data has been validated using the C-A fractal model for Cu anomalies associated with alteration zones (Afzal et al., 2015).

The purpose of this study is to characterize the spatial distributions of linear structures extracted from remote sensing images in vegetated areas, and to examine their possible relationships with the hydrothermal mineral deposits, using fractal and multifractal models in 2-D space.

1 STUDY AREA AND DATA

1.1 Geological Setting

Our study region is located in the Pinghe region, southern Fujian Province, and measures 1 408 km² (Fig. 1). The area is heavily vegetated and undulating in landform. The area hosts the Jurassic Lishan, Zhangpin, and Nanyuan groups, the Cretaceous Huangkeng and Zhaixia groups, and the Upper Jurassic granites and granite porphyries (Fig. 1). The strong Late Jurassic–Early Cretaceous Yanshanian tectonic movement produced widespread block structures, magmatic intrusions, and volcanic eruptions in the region. The Zhongteng volcanic structure, a circular structure located in the study area, is a part of a volcanic edifice formed during this period. The intrusive rocks are present either along the regional tectonic structures or along the center of volcano structures (center intrusions or center intrusive rock group) and circular radiated structures (circular intrusions or cyclic combination intrusive rock group). The magmatic intrusions, including the Zhongteng, Gushuang, Dingcheng, Ouliao, and Neiguoxi intrusions, are mostly complex and composed of mainly acid and intermediate-acidic rocks. The Jurassic Nanyuan Group, widely developed in this area, is mainly composed of intermediate-acid and acid conti-

mental volcanic eruptive rocks. It is an important ore-hosting horizon that contains a number of hydrothermal deposits, such as Zhongteng Cu-Mo deposit, Panchi Cu-Mo deposit, Xiaofanshan alunite deposit and other polymetallic mineralized points showing with green dot in Fig. 1. The study area experienced Yanshan and Himalayan multistage tectonic movements that affected the formed Fu'an-Nanjing and Shanghang-Yunxiao deep faults and formed several fault zones and fracture belts of different sizes and properties. The main faults in the study area, which provided the pathway for the hydrothermal fluids that produced the significant metal depositional sites (Shi and Wang, 2014; Zuo et al., 2013), have NW and NE orientations.

1.2 ETM+ Data

The ETM+ instrument carried by Landsat satellite records data in seven multispectral bands, including six bands in the visible and reflected infrared part of the electromagnetic spectrum and one channel in the thermal infrared region (Rajendran et al., 2012). The ETM+ data used in this study was obtained from the Computer Network Information Center, Chinese Academy of Sciences (<http://www.cnic.cn/zcfw/sjfw/gjksjxx/>), which was covered the entire study area. It was acquired on Feb. 28, 2002 with less than 2% cloud cover. The orbit number is p120/r42. It is georeferenced to the UTM projection and for the WGS-84 ellipsoid. The image was pretreated for geometric and radiometric corrections, band combination, and wavelet fusion based on IHS transformation. In order to optimize and enhance the visual effect, the 3-D visualization of remote sensing image was carried out based on software platform ArcGlobe10.0.

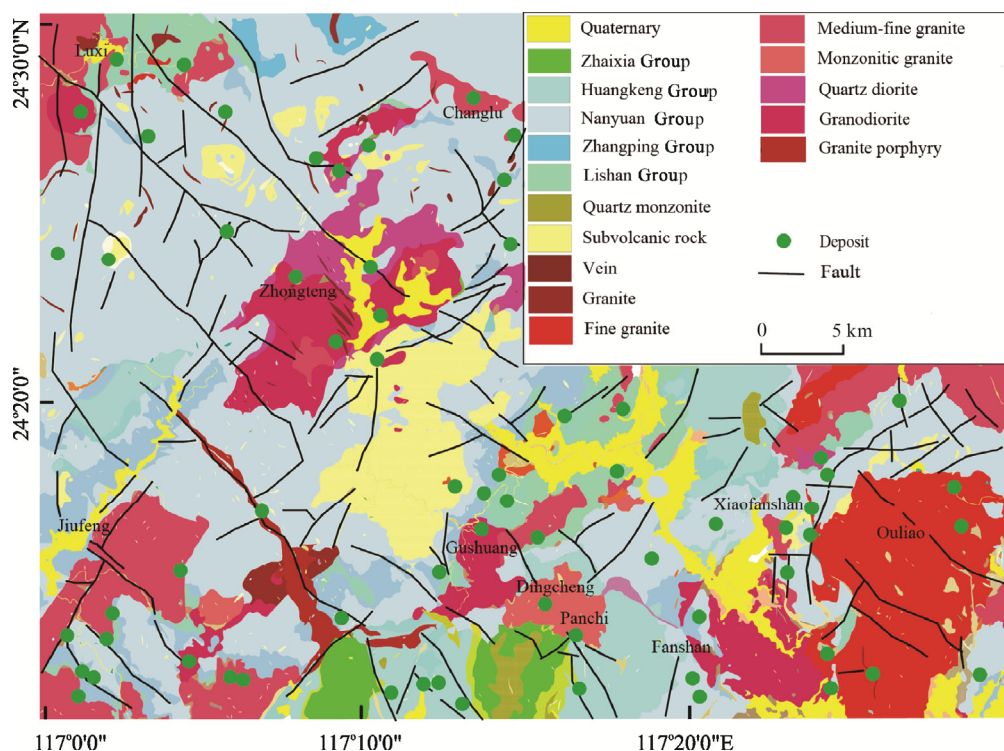


Figure 1. Simplified 1 : 50 000 geological map of Pinghe District (modified from Geological Survey Institute of Fujian, 2011).

1.3 Interpretation of Geological Structures from Remote Sensing Image

Mineral resources may be closely related with lineaments, which can be linear or circular structures, produced by geological processes (Du et al., 2014; Wei et al., 2010; Zhang et al., 2010; Chernicoff et al., 2002; Wang and Xu, 2002; Deng et al., 2000). The lineations in textures, tones, and terrains in the Pinghe District are studied based on the ETM+ data combined with the geological data. After linear stretching, filtering, and enhancement of the ETM+ data, combined with the DEM data, the 3-D visualization of the remote sensing image was created. The interpretation keys of lineaments in the derived 3-D image are various, such as red or magenta colored areas (Fig. 2d), which mainly indicate human activities and residential areas; blue colored areas (Fig. 2d), which show river systems; and landform texture (Fig. 2c), etc. The 3-D remote sensing images can provide different visual angles and distances of the region of interest, and can highlight the topography. Thus, 3-D remote sensing images allow us to observe the terrain characteristics of the study area more clearly than 2-D images, and allow us to make more accurate interpretations. Linear structures in the remote sensing image were interpreted using field data and geological maps (Fig. 4). The locations of some samples of interpretation for lineaments were showed in Fig. 4.

Linear structures on rock masses were formed depending on the lithospheric strength of the crust during the rock forma-

tion and deformation periods. Residential areas showed as relatively straight, continuous, stable lines, and occasionally extend more than a dozen kilometers (Fig. 2a). Human activities and several residential areas were found to be distributed around the river system located in the valley of the study area (Fig. 2d). As shown in Fig. 2d, the formation of the valley is mainly controlled by the presence of a fault, and the right-angle turn that forms in the Luxi District is also caused by a fault. The landform in the 3-D image shows that the valley is narrow and deep. The triangular facets of the fault are arranged in a continuous manner on both sides of the valley (Figs. 2b, 2c).

Circular structures in remote sensing image are ring features caused by rounded tectonic movement, magmatism, hydrothermal alteration, diffusivity of hydrocarbons, or thermal radiation, among others. Some of the circular structures in the remote sensing image are oval, pink, or magenta (Figs. 3a, 3b); these are tone abnormalities (Ran et al., 2010; Lana et al., 2008). Other abundant circular structures are small annular and oval structures, which are seen as smooth, fine-grained shadows. The typical negative terrain of a crater surrounded by mountains is also displayed in the 3-D image (Figs. 3a, 3b, 3c). Furthermore, there are abundant circular water systems around mountains (Figs. 3d, 3e, 3g, 3h), and the thermal band of ETM+ in Fig. 3f shown the distribution of thermal information which can help us to identify the geological structures by water systems and rock features.

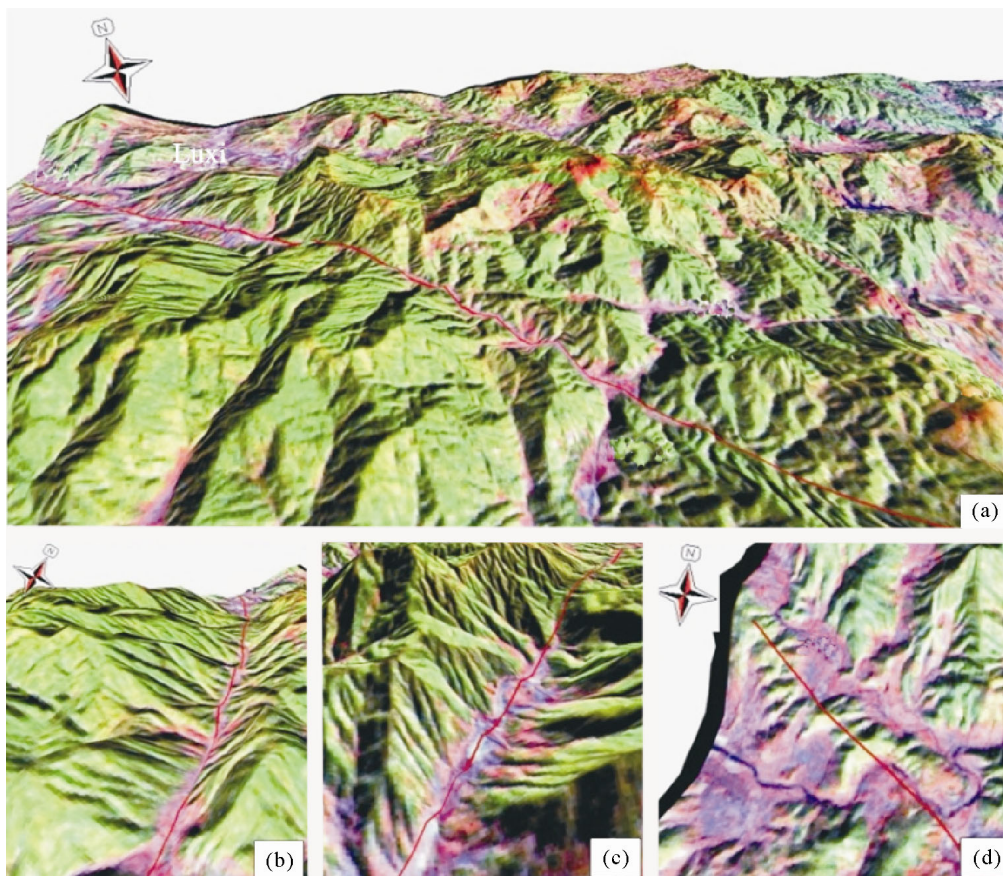


Figure 2. Samples of interpretation keys for lineaments in the 3-D image.

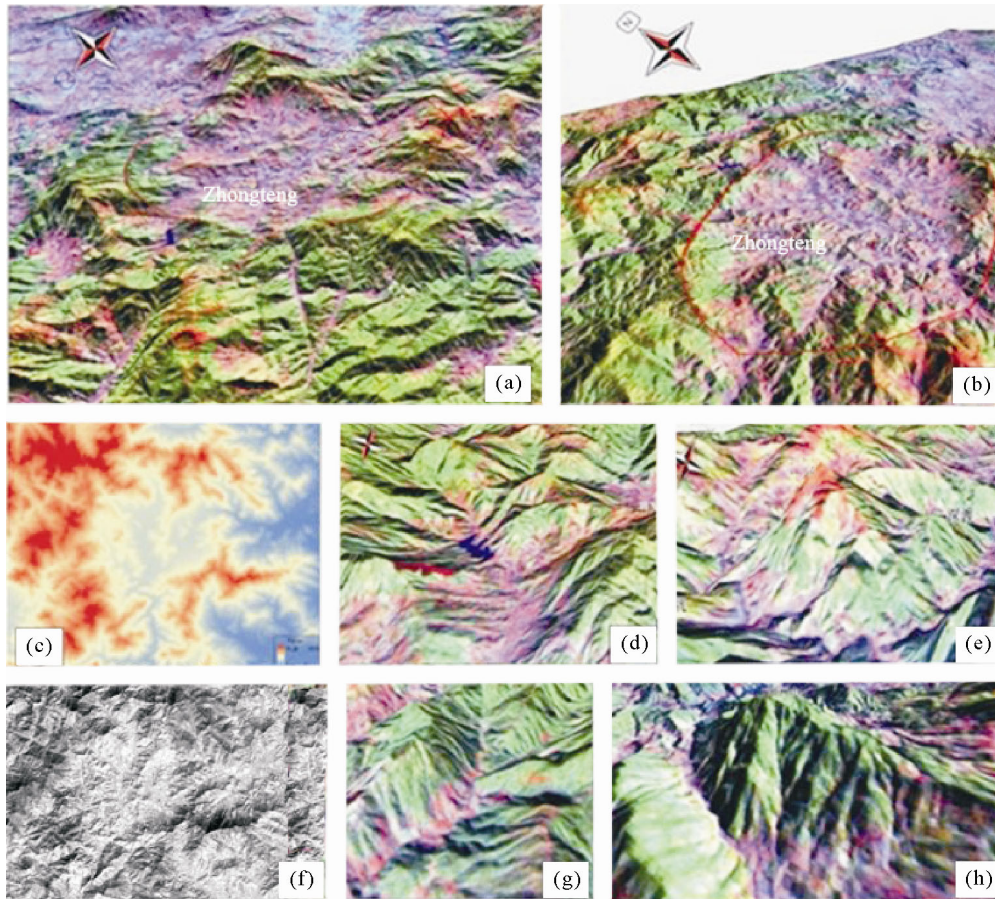


Figure 3. Samples of interpretation keys for circular structures in the 3-D image.

2 METHODOLOGY

2.1 Box-Counting Fractal Model

Fractal models are very useful tools for describing complicated physical processes and their end-production (Cheng, 2003, 2000). The scale invariance and the self-similarity properties of many physical processes and their end-production can be described by power-law models (Zhao J N et al., 2011). One way to obtain the fractal dimension is the box-counting method (Zuo and Xia, 2009; Zuo et al., 2009; Jiang, 2005; Pérez-López et al., 2005; Borodich, 1997; Walsh and Watterson, 1993; Velde et al., 1990) that can show a power-law relationship between the cumulative number and the cumulative size of similarly shaped objects in a log-log graph. When all the extracted lineations in the study are covered in a raster map with varying cell sizes, the box-counting relationship can be expressed as

$$N(r) \propto kr^{-D} \quad (1)$$

where r is a measure of unit size, $N(r)$ is the cumulative number of cells containing lineations, D is a box-counting fractal dimension, \propto represents a proportionality, and k is a constant. The D is obtained as the slope coefficient of linear regression between values of r and $N(r)$. The value of D varies between 1 and 2 for a two-dimensional map (Mandelbrot, 1983).

2.2 Spectrum-Area (S-A) Fractal Model

Cheng et al. (1994) proposed the petrogeochemistry “density-area (C-A)” fractal model concerning the relation

between concentration value (ρ) and the area (A) enclosed by contour value ρ . It can be expressed as

$$A(\rho \leq v) \propto \rho^{-a_1}; A(\rho > v) \propto \rho^{-a_2} \quad (2)$$

where $A(\rho)$ denotes the area enclosed by a contour value ρ ; v is a concentration threshold defining contour ρ ; a_1 and a_2 are fractal dimensions greater than zero, which can be estimated from slopes of straight lines fitted by least-squares method to a log-log plot of $A(\rho)$ versus ρ ; \propto represents a proportionality. Cheng (1999) extended the C-A model to the S-A model to describe the spectral energy density-area relationship in the frequency domain, which can be expressed as

$$A(\geq S) \propto S^{-2d/\beta} \quad (3)$$

where S represents the spectral energy density as a function of the wave number vector, $A[\geq S]$ denotes area in units of the wave number with a threshold above S , β is an anisotropic scaling exponent, d is a parameter representing the degree of overall concentration, and \propto represents proportionality.

Based on a power-law function derived from 2D linear generalized scale invariance (GSI), the S-A model represents the relationships between areas of data sets consisting of wave numbers with spectral energy density above $S[A(>S)]$ in 2D frequency domain. A spatial pattern can be decomposed into multiple components based on distinct anisotropic scaling properties in the frequency domain using this model (Zuo et al., 2013).

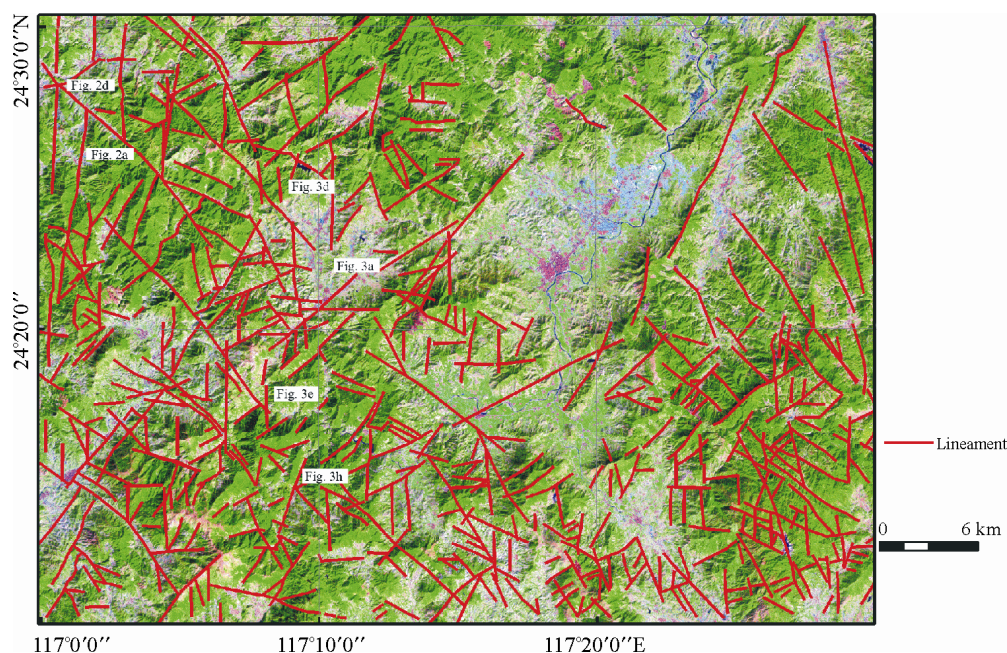


Figure 4. Mapped lineations (red polylines) in Pinghe District.

3 RESULTS AND DISCUSSION

3.1 Fractal Dimensions of Lineament Patterns

The study area was divided into 30×40 square cells. The fractal dimension D in every cell is calculated by box-counting method. The analysis was carried out separately for the map of all lineations and for the maps of NW- and NE-trending lineations. The fractal dimensions in each of the four hydrothermal ore fields (i.e., Zhongteng, Panchi, Xiaofanshan and Fanshan) were calculated.

The value of D for all lineaments, NW-trending lineaments, and NE-trending lineaments are 1.36, 1.32, and 1.23, respectively (Table 1). The NW-trending lineaments are more abundant than the NE-trending lineaments. The spatial distributions of lineaments in the study area are statistically self-similar. The zones displaying high indices for fractal dimensions are mainly located nearby Zhongteng volcanic edifice, Dingcheng intrusive rocks and Ouliao intrusive rocks. The fractal dimensions of spatial distributions of lineaments in the two Cu-Mo deposits are 1.43 (Zhongteng) and 1.52 (Panchi) (Table 1). The fractal dimensions of spatial distributions of lineaments in the two alunite deposits are 1.37 (Xiaofanshan) and 1.37 (Fanshan). The four known ore deposits in the study area are located in zones with high fractal dimensions. The value of D for the map of all lineaments and the value of D for four hydrothermal ore deposits are higher than the fractal dimension value of the lineations in South China (1.35). The fractal dimension value of the lineations in the Dexing porphyry copper ore field and in the Gaolong gold deposit are 1.60 and 1.66, respectively (Table 1). The fractal dimensions of the study area indicate that the faults have a more complex structure and stronger activity in the four ore deposits.

The contour map of the fractal dimensions of the study area shows that the fractal dimension of lineaments is closely related to the number of lineaments. The analysis of the fractal dimensions in each cell suggests that higher numbers and

Table 1 Fractal characteristics of lineations in the study and other area

Area	Fractal dimension	Source of data
All lineations	1.36	This study
The NW lineations	1.32	This study
The NE lineations	1.23	This study
Zhongteng Cu-Mo field	1.43	This study
Panchi Cu-Mo field	1.52	This study
Xiaofanshan alum field	1.37	This study
Lineations in South China	1.35	Kong and Ding, 1991
Dexing porphyry copper ore field	1.60	Jin et al., 1998
Gaolong gold deposit	1.66	Yu and Yuan, 2005

densities of lineaments correspond to higher fractal dimensions (Fig. 5). In addition, the area with high fractal dimensions is more conducive to mineralization in the contour map.

3.2 Tendency Characteristics of Fractal Dimensions of Lineations.

Trend analysis shows that the zones with high fractal dimensions correlate well with the deep fault and the volcanic edifice in the high step tendency maps of the fractal dimensions, indicating possibly the boundary of the volcanic edifice and the deep fault controlling the development of the rock mass and the volcanic edifice.

The high step tendency maps of the fractal dimensions of lineations showed that the zones with high indices generally exhibit NW and NE orientations, especially in the 8-step tendency map (Fig. 6). The NE-trending zone with high indices shown in the 10-step tendency map is coincident with the deep fault located in Jiufeng, and the NW-trending zone with high indices in the map is consistent with the fault near the Panchi Cu-Mo deposit.

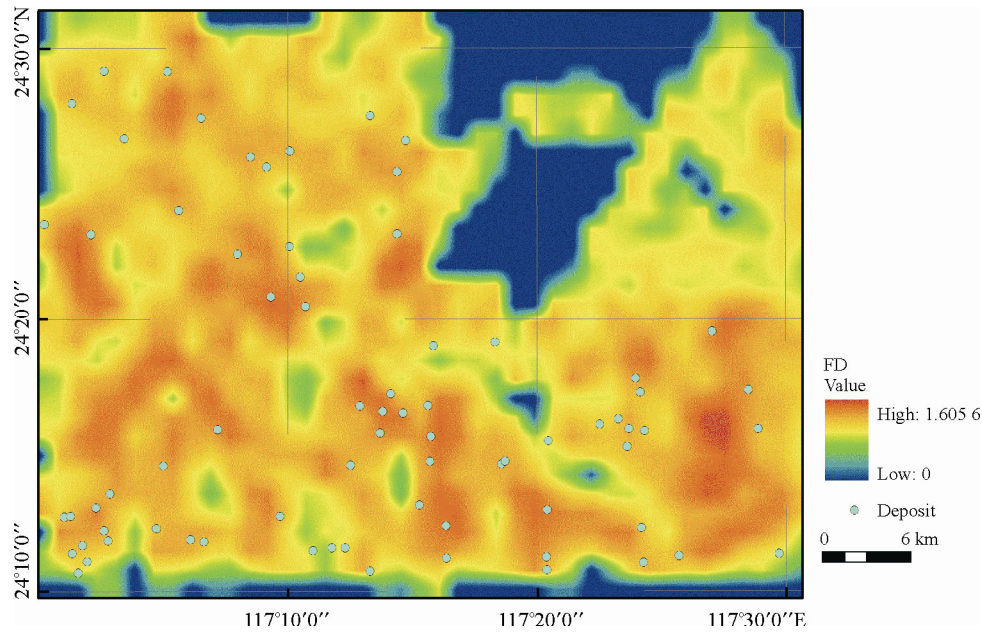


Figure 5. The contour map of the fractal dimensions for the lineations in the study area.

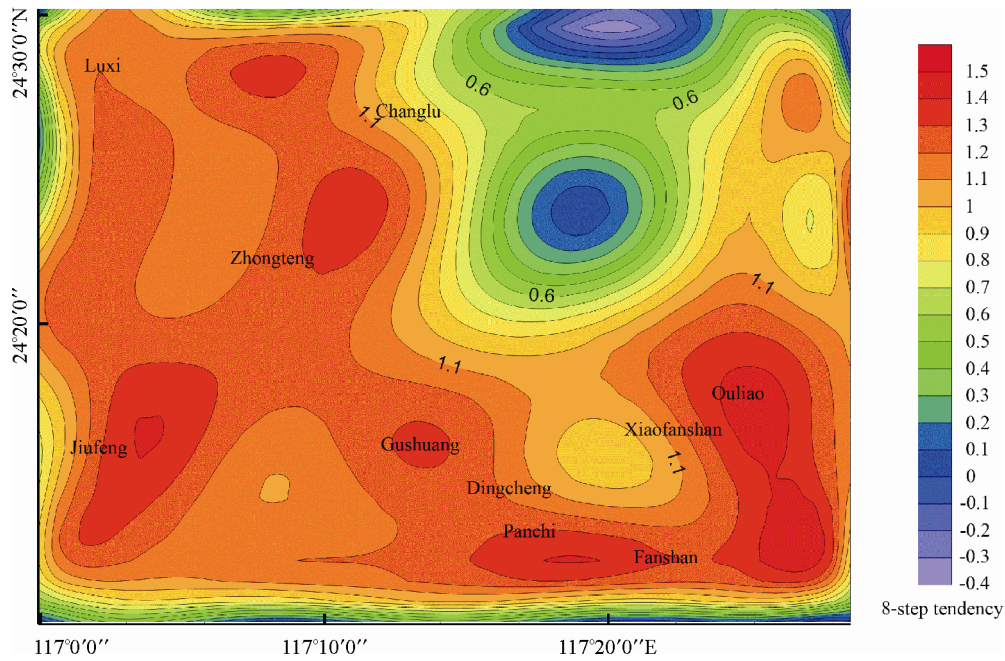


Figure 6. The 8-step tendency map of the fractal dimensions for the lineations in the study area.

In addition, there is an annular region with high indices in the 10-step tendency map that is coincident with the Zhongteng circular structure in the ETM+ image (Fig. 7), which corresponds to the largest caldera in the study area. Moreover, the area with high indices situated in the Ouliao circular structure correlates well with Ouliao intrusive rocks.

3.3 S-A Fractal Model Application.

The S-A fractal model based on the power-law relationships between areas of data sets, is a useful tool to decompose the mixed spatial pattern and non-linear imaging processing (Zuo, 2011a, b; Cheng et al., 2010; Zuo and Xia, 2009). Fourier Transformation (FT) is used to convert the spatial pattern of

fractal dimensions contour map into the frequency domain. In this study, 500 samples were used to produce R^2 and two components were obtained consisting of power spectrum density and phase. The spectrum density (S) and the number cells with greater than or equal to S were plotted in a log-log graph. Three straight lines with two cutoff values were obtained by using the least squares (LS) method, which can be fitted using these pairs of data components. The cutoff values $\ln S=2.80$ and 3.90 were used to define three filters: one consists of wave numbers with $\ln S \leq 2.80$ as the noise filter, wave numbers with $2.80 < \ln S < 3.90$ as the anomaly filter and $\ln S \geq 3.9$ as the background filter (Cheng et al., 2010). In other word, the left-hand line ($\ln S \leq 2.80$) gives $y = -0.65x + 3.76$ ($R^2=0.98$) and

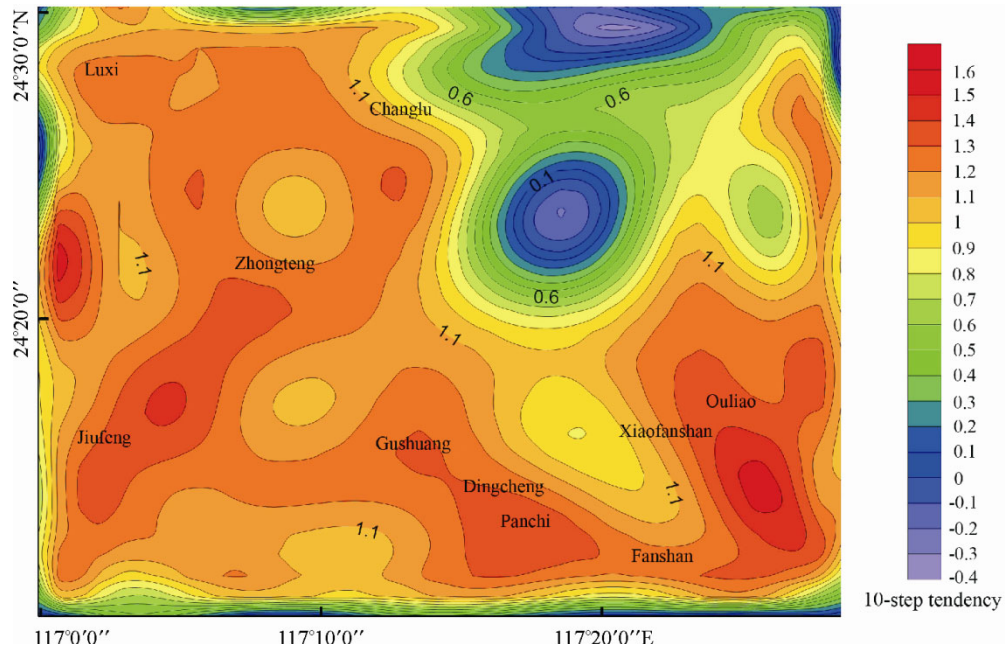


Figure 7. The 10-step tendency map of the fractal dimensions for the lineations in the study area.

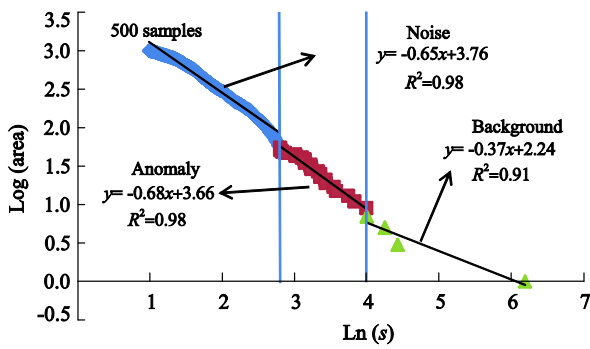


Figure 8. Threshold segmentation of calculation of S-A fractal model.

represents the noise. The middle line ($2.80 < \ln S < 3.90$) represents the anomaly, which gives $y = -0.68x + 3.66$ ($R^2 = 0.98$). The right-hand line ($\ln S \geq 3.90$) is for background and gives $y = -0.37x + 2.24$ ($R^2 = 0.91$) (Zuo et al., 2013; Cheng et al., 2010). We used inverse Fourier transformed functions (IFT) to convert these three frequency components back into the spatial domain. We were interested in the anomaly map, which is shown in Fig. 8.

The anomaly map (Fig. 9) decomposed by S-A fractal model shows that most of the known hydrothermal deposits occur in the high anomalous area much more clearly than the

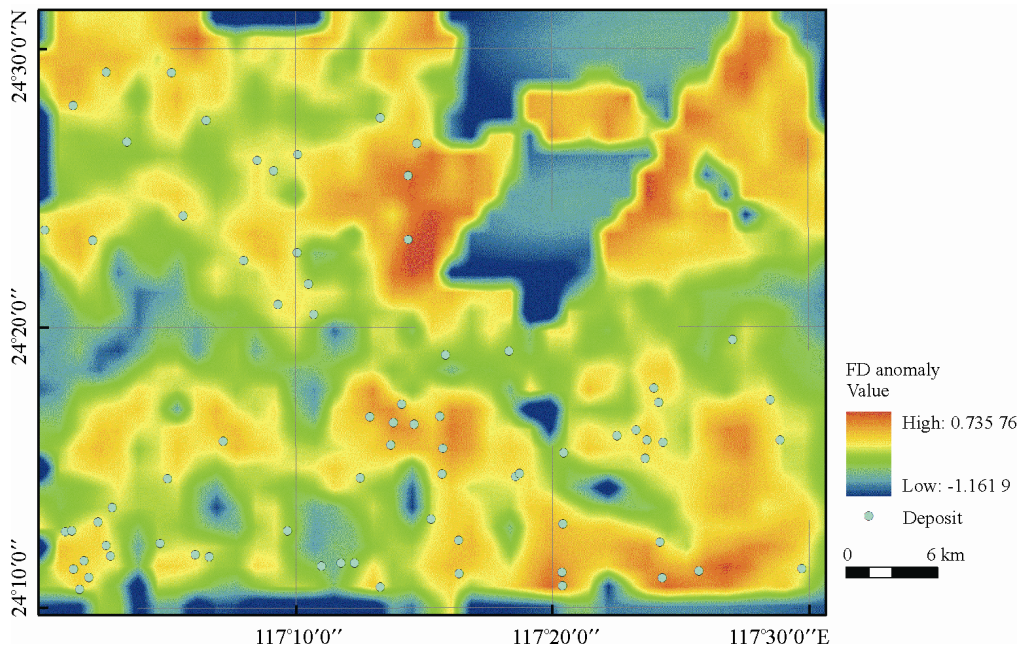


Figure 9. The decomposed anomaly map for the contour map of the fractal dimensions.

original fractal dimensions contour map. That is to say, the anomalous areas are spatially in good agreement with the locations of known hydrothermal deposits and mineralized points. The fact that the hydrothermal deposits are located in the high anomalous area suggests that the faults probably provided the pathway for hydrothermal fluids that produced the significant metal depositional sites. The Nanyuan Group, which is cut by abundant faults, was also affected by the hydrothermal polymetallic ore mineralization.

4 CONCLUSIONS

This study established the 3-D image and summarized the interpretation keys of linear ring structure, which improved the precision and accuracy of linear ring structural interpretation in vegetation coverage area. The result shows that fractal properties of the mapped lineations in the Pinghe vegetated area are closely related with the spatial distribution of linear structures and hydrothermal ore deposits. Considering that the contour map of the fractal dimensions of the linear structures extracted in the ETM+ image (3-D image) exhibited fractal characteristics and statistical self-similarity, the spatial distribution of mapped lineations could be described by the fractal modelling.

The following fractal properties, which can be used to find ore deposits and interpret deep structures in other intensely vegetated areas, have been observed in this study: 1) the hydrothermal ore deposits are mostly located in zones with high fractal dimensions shown in the fractal dimensions contour map; 2) the high step tendency maps of the fractal dimensions show the boundary of the volcanic edifice and the deep fault that controls the development of the rock mass and the volcanic edifice; 3) most of the hydrothermal ore deposits are located around high anomalous areas on the map decomposed by the spectrum-area (S-A) multifractal model, which is more clearly than the original fractal dimensions contour map; 4) the faults probably provided the pathway for hydrothermal fluids and determined the sites for hydrothermal ore mineralization in this study area.

ACKNOWLEDGMENTS

The authors thank two anonymous reviewers for their critical comments. The authors are very grateful to Guoxiong Chen for his help and constructive comments. This research was supported by the “Quantitative Models for Prediction of Strategic Mineral Resources in China” (No. 201211022) by the Ministry of Land and Resources of China and “Integrated Prediction Theory for Mineral Resource in Desert and Grassland Covered Areas and Geoinformation Extraction of Buried Mineral Resource” (No. 41430320) by the National Natural Science Foundation of China. The final publication is available at Springer via <http://dx.doi.org/10.1007/s12583-016-0914-x>.

REFERENCES CITED

- Afzal, P., Aramesh Asl, R., Adib, A., et al., 2015. Application of Fractal Modelling for Cu Mineralisation Reconnaissance by ASTER Multispectral and Stream Sediment Data in Khoshname Area, NW Iran. *Journal of the Indian Society of Remote Sensing*, 43(1): 121–132. doi:10.1007/s12524-014-0384-6
- Aramesh Asl, R., Afzal, P., Adib, A., et al., 2015. Application of Multifractal Modelling for the Identification of Alteration Zones and Major Faults Based on ETM+ Multispectral Data. *Arabian Journal of Geosciences*, 8(5): 2997–3006. doi:10.1007/s12517-014-1366-2
- Borodich, F. M., 1997. Some Fractal Models of Fracture. *Journal of the Mechanics and Physics of Solids*, 45(2): 239–259. doi:10.1016/s0022-5096(96)00080-4
- Carlson, C. A., 1991. Spatial Distribution of Ore Deposits. *Geology*, 19(2): 111–114 doi:10.1130/0091-7613(1991)019<0111:sdood>2.3.co;2
- Cheng, Q. M., 1999. Multifractal Interpolation. In: Lippard, S. J., Naess, A., Sinding-Larsen, R., eds.. Proceedings of the Fifth Annual Conference of the International Association for Mathematical Geology, Vol. 1, Trondheim, Norway. 245–250
- Cheng, Q. M., 2000. Multifractal Theory and Geochemical Element Distribution Pattern. *Earth Science—Journal of China University of Geosciences*, 25(3): 311–318 (in Chinese with English Abstract)
- Cheng, Q. M., 2003. Fractal and Multifractal Modeling of Hydrothermal Mineral Deposit Spectrum: Application to Gold Deposits in Abitibi Area, Ontario, Canada. *Journal of China University of Geosciences*, 14(3): 199–206
- Cheng, Q. M., Agterberg, F. P., Ballantyne, S. B., 1994. The Separation of Geochemical Anomalies from Background by Fractal Methods. *Journal of Geochemical Exploration*, 51(2): 109–130. doi:10.1016/0375-6742(94)90013-2
- Cheng, Q. M., Agterberg, F. P., Bonham-Carter, G. F., 1996. A Spatial Analysis Method for Geochemical Anomaly Separation. *Journal of Geochemical Exploration*, 56(3): 183–195. doi:10.1016/s0375-6742(96)00035-0
- Cheng, Q. M., Xia, Q. L., Li, W., et al., 2010. Density/Area Power-Law Models for Separating Multi-Scale Anomalies of Ore and Toxic Elements in Stream Sediments in Gejiu Mineral District, Yunnan Province, China. *Biogeosciences*, 7(10): 3019–3025. doi:10.5194/bg-7-3019-2010
- Chernicoff, C. J., Richards, J. P., Zappettini, E. O., 2002. Crustal Lineament Control on Magmatism and Mineralization in Northwestern Argentina: Geological, Geophysical, and Remote Sensing Evidence. *Ore Geology Reviews*, 21(3): 127–155. doi:10.1016/s0169-1368(02)00087-2
- Deng, Q. L., Wang, X. P., Liu, J. P., et al., 2000. Relations between Landslide and Lineament in the Lower Part of the Three Gorges, Yangtze River. *Journal of Changchun University of Science and Technology*, 30(4): 384–387 (in Chinese with English Abstract)
- Du, W. H., Wang, G. W., Chen, Y. Q., et al., 2014. Information Extraction and Interpretation Analysis of Mineral Potential Targets Based on ETM+ Data and GIS technology: A Case Study of Copper and Gold Mineralization in Burma. 35th International Symposium on Remote Sensing of Environment (ISRSE35), IOP Conf. Series. *Earth and Environmental Science*, 17(1): 012175. doi:10.1088/1755-1315/17/1/012175
- Gumiel, P., Sanderson, D. J., Arias, M., et al., 2010. Analysis of the Fractal Clustering of Ore Deposits in the Spanish Iberian Pyrite Belt. *Ore Geology Reviews*, 38(4): 307–318. doi:10.1016/j.oregeorev.2010.08.001
- Jiang, W. D., 2005. Fractal Character of Lenticles and Its Influence on Sediment State in Tailings Dam. *Journal of Central South University—Science and Technology*, 12(6): 753–756 (in Chinese with English Abstract)
- Jin, Z. D., Lu, X. W., Zhang, C. L., 1998. A Study of Fractal Dimension of the Fracture System in the Dexing Porphyry Copper Orefield, Jiangxi. *Geological Review*, 44(1): 57–62 (in Chinese with English Abstract)
- Ke, X. Z., Xie, S. Y., Zheng, Y. Y., et al., 2015. Multifractal Analysis of Geochemical Stream Sediment Data in Bange Region, Northern Tibet.

- Journal of Earth Science*, 26(3): 317–327. doi:10.1007/s12583-015-0538-7
- Kong, F. C., Ding, G. Y., 1991. The Implications of the Fractal Dimension Values of Lineaments. *Earthquake*, 10(5): 33–37 (in Chinese with English Abstract)
- Lana, C., Souza Filho, C. R., Marangoni, Y. R., et al., 2008. Insights into the Morphology, Geometry, and Post-Impact Erosion of the Araguainha Peak-Ring Structure, Central Brazil. *Geological Society of America Bulletin*, 119(9): 1135–1150. doi:10.1130/b26142.1
- Ma, Y. L., Xu, R. S., 1999. Application of Remote Sensing and Biogeochemistry to Prospecting and Their Practical Results. *Geology and Prospecting*, 35(5): 39–42 (in Chinese with English Abstract)
- Mandelbrot, B. B., 1983. *The Fractal Geometry of Nature* (Updated and Augmented Edition). W. H. Freeman and Company, New York. 495
- Pérez-López, R., Paredes, C., Muñoz-Martín, 2005. Relationship between the Fractal Dimension Anisotropy of the Spatial Faults Distribution and the Paleostress Fields on a Variscan Granitic Massif (Central Spain): The F-Parameter. *Journal of Structural Geology*, 27(4): 663–677. doi:10.1016/j.jsg.2005.01.002
- Rajendran, S., Al-Khribash, S., Pracejus, B., et al., 2012. ASTER Detection of Chromite Bearing Mineralized Zones in Semail Ophiolite Massifs of the Northern Oman Mountains: Exploration Strategy. *Ore Geology Reviews*, 44(2): 121–135. doi:10.1016/j.oregeorev.2011.09.010
- Ran, L., Liu, Z. T., Yang, Z. A., et al., 2010. Analysis of Structural Image Characteristics in the Kalatage Area, Eastern Xinjiang. *Geology and Exploration*, 46(6): 1099–1105 (in Chinese with English Abstract)
- Shi, C., Wang, X. P., 2014. Extraction of Remote Sensing Anomaly of Geological Structure and Ore Prediction in Vegetation Coverage in Fujian. *Journal of Geology*, 38(3): 464–469 (in Chinese with English Abstract)
- Velde, B., Dubois, J., Touchard, G., et al., 1990. Fractal Analysis of Fractures in Rocks: The Cantor's Dust Method. *Tectonophysics*, 179(3/4): 345–352. doi:10.1016/0040-1951(90)90300-w
- Walsh, J. J., Watterson, J., 1993. Fractal Analysis of Fracture Patterns Using the Standard Box-Counting Technique: Valid and Invalid Methodologies. *Journal of Structural Geology*, 15(12): 1509–1512. doi:10.1016/0191-8141(93)90010-8
- Wang, L. Q., Xu, G., 2002. Characteristics of Major Linear Structures Shown by ETM Data of the Geermu-Tanggula Mountain Pass Section along the Qinghai-Xizang Railway. *Acta Geoscientia Sinica*, 23(4): 349–352 (in Chinese with English Abstract)
- Wei, G. J., Gao, J. G., Yang, S. Y., et al., 2010. A Study on the Linear and Circular Structure Interpretation and Prospecting in the Lancang Area using Remote Sensing Image. *Mine Surveying*, 10(6): 8–10 (in Chinese with English Abstract)
- Yu, Y., Yuan, A. P., 2005. Quantitative Analysis with High Resolution Remote Sensing Lineament in Gaolong Gold Deposit. *Guangxi Sciences*, 12(3): 200–202 (in Chinese with English Abstract)
- Zhang, W., Yang, J. Z., Fang, H. B., et al., 2010. Remote Sensing Interpretation and Metallogenic Prediction in the Metallogenic Belts of East Kunlun and Altun Mts. *Northwestern Geology*, 43(4): 288–294 (in Chinese with English Abstract)
- Zhao, J. N., Chen, S. Y., Zuo, R. G., et al., 2011. Mapping Complexity of Spatial Distribution of Faults Using Fractal and Multifractal Models: Vectoring towards Exploration Targets. *Computers & Geosciences*, 37(12): 1958–1966. doi:10.1016/j.cageo.2011.04.007
- Zhao, S., Qian, J., Chen, H., 2011. Application of Fractal Statistics of Linear Structure and Alteration Information Extraction of Remote Sensing on the Au, Pb, Zn, Sn Polymetallic Mineralogenetic Prognosis in Eastern Guangxi. *Geotectonica et Metallogenia*, 35(3): 364–371 (in Chinese with English Abstract)
- Zuo, R. G., 2011a. Decomposing of Mixed Pattern of Arsenic Using Fractal Model in Gangdese Belt, Tibet, China. *Applied Geochemistry*, 26(3): S271–S273. doi:10.1016/j.apgeochem.2011.03.122
- Zuo, R. G., 2011b. Identifying Geochemical Anomalies Associated with Cu and Pb-Zn Skarn Mineralization Using Principal Component Analysis and Spectrum-Area Fractal Modeling in the Gangdese Belt, Tibet (China). *Journal of Geochemical Exploration*, 111(1–2): 13–22. doi:10.1016/j.gexplo.2011.06.012
- Zuo, R. G., Agterberg, F. P., Cheng, Q. M., et al., 2009. Fractal Characterization of the Spatial Distribution of Geological Point Processes. *International Journal of Applied Earth Observation and Geoinformation*, 11(6): 394–402. doi:10.1016/j.jag.2009.07.001
- Zuo, R. G., Cheng, Q. M., Xia, Q. L., et al., 2008. Application of Fractal Models to Distinguish between Different Mineral Phases. *Mathematical Geosciences*, 41(1): 71–80. doi:10.1007/s11004-008-9191-3
- Zuo, R. G., Xia, Q. L., 2009. Application Fractal and Multifractal Methods to Mapping Prospectivity for Metamorphosed Sedimentary Iron Deposits Using Stream Sediment Geochemical Data in Eastern Hebei Province, China. *Geochimica et Cosmochimica Acta*, 73(13): 827–833
- Zuo, R. G., Xia, Q. L., Wang, H. C., 2013. Compositional Data Analysis in the Study of Integrated Geochemical Anomalies Associated with Mineralization. *Applied Geochemistry*, 28(28): 202–211. doi:10.1016/j.apgeochem.2012.10.031